IMEKO 20th TC3, 3rd TC16 and 1st TC22 International Conference
Cultivating metrological knowledge
27th to 30th November, 2007. Merida, Mexico.

Development of Shock Acceleration Calibration Machine in NMIJ

Hideaki Nozato, Takashi Usuda, Akihiro Oota, Tamio Ishigami and Katsuhisa Kudo

National Metrology Institute of Japan, Advanced Industrial Science and Technology

Abstract

Calibrations of shock acceleration are industrially required from a view of human safety and product development. In NMIJ vibration group, a shock acceleration calibration machine (hereafter 'calibration machine') has been developed in response to much demand from Japanese industries, and can calibrate shock transducers in acceleration range from 200 m/s^2 to 5000 m/s^2. For primary calibration, accelerometer is calibrated by a combination of shock exciter and laser interferometer. In the shock exciter, shock acceleration is generated by rigid body collision between a hammer and an anvil. To avoid any disturbance motion, radial air bearing system is adapted to keep high stiffness in perpendicular directions to the collision. The hammer, supported by the air bearing, is accelerated by an air gun and collides with the anvil through a rubber pad. Thus, acceleration waveform of the anvil strongly depends on viscoelasticity of the rubber pad. Different hardness of the rubber pad is examined to realize various peak accelerations. As another significant issue, optimization of low-pass digital filter is necessary to obtain reliable acceleration waveforms. This manuscript reports not only a procedure of low-pass digital filtering but also cut-off frequency dependence of low-pass digital filter on peak acceleration.

Keywords: acceleration standard, shock acceleration, air bearing, accelerometer, calibration, low-pass digital filter

1. Introduction

Precise and reliable acceleration measurement is industrially required from a view of human safety and product development. In NMIJ vibration group, accelerometers have been calibrated in range from 1 m/s^2 to 100 m/s^2 with 0.1 Hz to 5 kHz [1]. We have had an effort to expand the amplitude and frequency of vibration in response to demand flexibly. However, especially in automobile field, above acceleration range

is not sufficient for their demand. For example, in case of car collision test, some safety criteria are regulated among Japanese, European and American government agencies. As a typical threshold, maximum acceleration acting at driver's chest must be less than 588 m/s^2 when a car with speed of 50 km/h collides with hard wall [2]. Since enormous resource and time are consumed in car collision test, it is beneficial to develop shock acceleration standard in NMIJ and supply it to Japanese industries. For such a purpose, the targeted range of shock acceleration should cover, at least from 200 m/s^2 to 5000 m/s^2.

International Standard ISO 16063-13 [3] describes two methods for primary calibration of shock transducers, using collision motion between two rigid bodies, and using propagation wave in steel bar. For shock acceleration from 200 m/s^2 to 5000 m/s^2, we adapt the method using collision motion between two rigid bodies. Displacement of a transducer fixed to the collided rigid body is measured by a modified Michelson laser interferometer, and acceleration of the transducer is derived through two numerical differentiations and two low-pass digital filtering from the displacement. This manuscript reports calibration principle, specification of shock acceleration, and low-pass digital filtering effect.

2. Shock Acceleration Calibration Machine

2.1 Shock Exciter

Figure 1 shows schema of the calibration machine in NMIJ. The calibration machine mainly consists of shock exciter and laser interferometer.

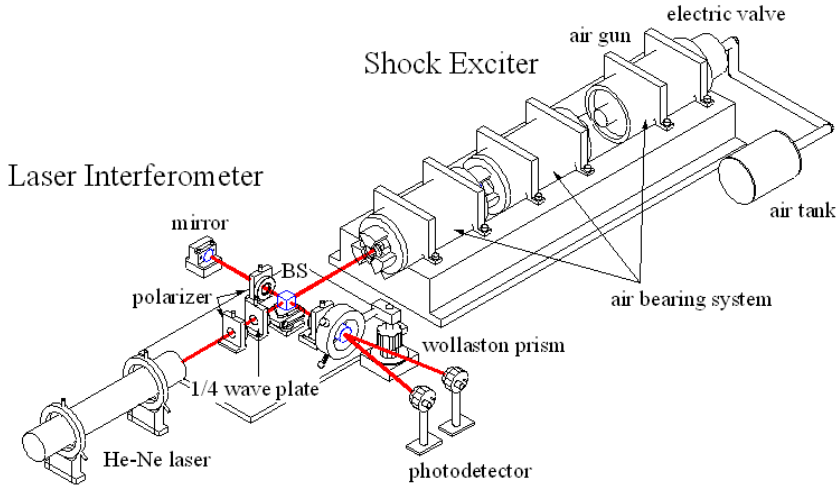

Figure 1 Schema of shock acceleration calibration machine

In Fig. 2, structure of the shock exciter in the calibration machine is drawn.

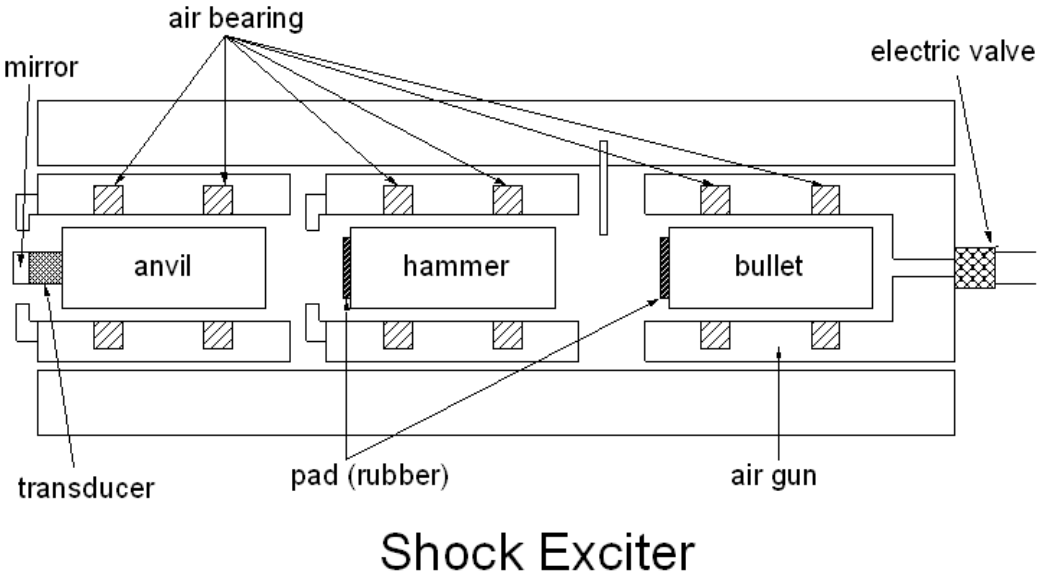

Figure 2 Structure of shock exciter.

The shock exciter has three movable parts, so called bullet, hammer and anvil. Each movable part is supported by two radial air bearings, which sustain spatial space of 10 μm in the radial direction. Material of the hammer and the bullet is stainless steel, and that of the anvil is stainless steel or aluminum. Each movable part is cylindrical shape with a diameter of 30 mm and a length of 200 mm, and equips a transducer or a rubber pad on one end surface as indicated in Fig. 2. The air bearing has circular structure with an internal diameter of 30 mm. The anvil, the hammer and the bullet move with very low friction inside the air bearing. Velocity of the hammer and the bullet, which weigh the same, is given by a combination of opening time of the electric valve and air pressure in air tank. To make hammer velocity accelerate up to 3 m/s, the specifications such as electric valve, air pressure (0.2 MPa to 0.6 MPa) and air tube are designed. If hammer velocity is given as an initial condition, acceleration waveform of the anvil depends on anvil mass and viscoelasticity of the rubber pad which is set up between the anvil and the hammer.

As cited above, a transducer is attached on one end surface of the anvil. Here, accelerometer consists of the transducer (BK8305) and a charge amplifier (BK2525). It is well known that the accelerometer has reliable sensitivity with good phase characteristic.

2.2 Laser Interferometer and Equipment Devices

Laser interferometer of the calibration machine is a modified Michelson laser interferometer for quadrature signals [$u_1(t)$ and $u_2(t)$], and is set up on the same vibration-isolation table together with the shock exciter. Length standard is a wavelength of 632.8 nm in a stabilized He-Ne laser, built in the laser interferometer. Additionally, two digitizers (Gage, Compuscope 12100) and analysis program (Labview) are provided as equipment devices. The two digitizers with four channels store time-series signal of quadrature signals and accelerometer output, and then transfer them to the analysis program. Maximum sampling rate and vertical resolution are 50 MS/s and 12 bit for each channel. Figure 3 presents a typical example of P-polarized and S-polarized component in quadrature signals.

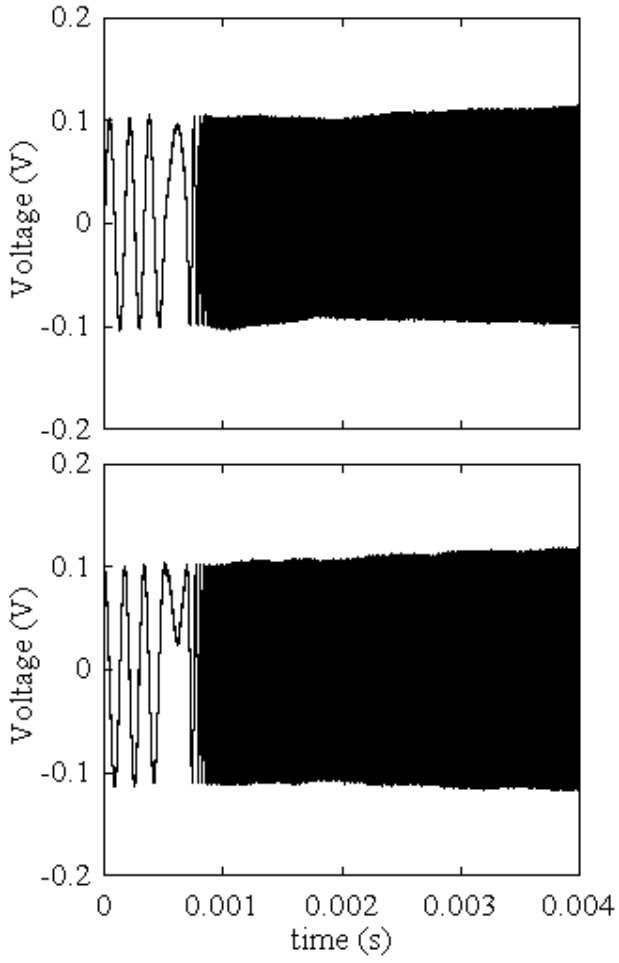

Figure 3 Example of P-polarized and S-polarized component in qudrature signals.

After the quadrature signals are corrected to be a circular shape in X-Y coordinate

[4], displacement *s*(*t*) is derived from phase unwrapping method using following equations described in ISO 16063-13.

$$\varphi(t) = \arctan\frac{u_2(t)}{u_1(t)} + n\pi \ . \tag{1}$$

$$s(t) = \frac{\lambda}{4\pi}\varphi(t) \ . \tag{2}$$

Finally in the analysis program, the displacement signal is transformed to acceleration signal through two numerical differentiations and two low-pass digital filtering.

3. Low-pass Digital Filtering Effect, and Specification of Shock Acceleration

Figure 4 (a) and (b) shows accelerometer output (AO) and demodulated acceleration (DA) under the experimental data in Fig. 3. Here, 4th order Butterworth low-pass filter with a cut-off frequency of 5 kHz is selected as a low-pass digital filter. In order to investigate how the low-pass digital filter affects phase of signals, two procedures are implemented. One is as follows. After time-series signal is forward filtered in time direction, the filtered time-series signal is backward filtered. We refer to this procedure as 'forward-backward filtering'. Another procedure, in which time-series signal is forward filtered twice in time direction, is referred as 'forward-forward filtering'. In Fig. 4 (a), thick line and thin dashed line stand for accelerometer output with forward-backward and forward filtering. Thin line means original accelerometer output. We consider that it is approximate to true acceleration waveform. If only forward filtering is applied to the original accelerometer output, phase delay arises in the filtered accelerometer output (thin dashed line). However, phase delay is compensated in case of forward-backward filtering.

More significant phase delay is observed in Fig. 4 (b) between forward-backward and forward-backward filtering, arising in each numerical differentiation process. Compared with the original accelerometer output (Fig. 4 (a) thin line), we consider that forward-backward filtering compensates phase delay in filtering process. As a result, peak position in time between accelerometer output (Fig. 4 (a) thick line) and demodulated acceleration (Fig. 4 (b) thick line) is agreed within 1 μs in this case. To keep consistency of phase characteristic in both accelerometer output and demodulated acceleration, comparable filtering process (forward-backward filtering) shall be employed for both evaluations.

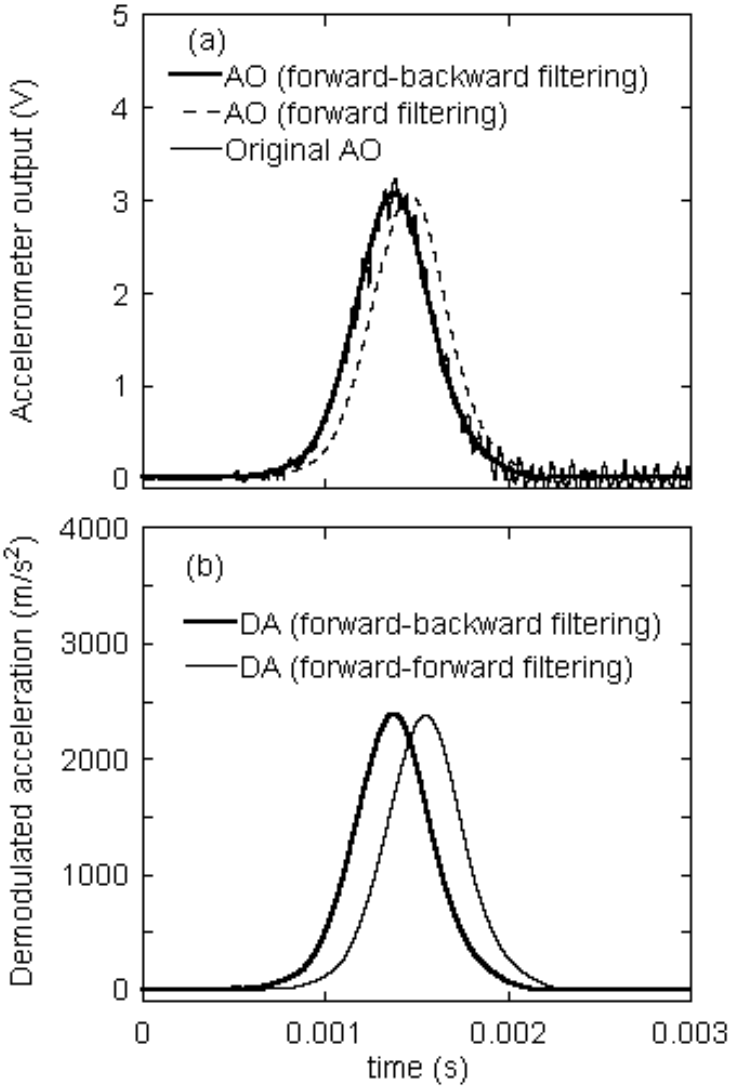

Figure 4 Example of (a) accelerometer output and (b) demodulated acceleration.

Figure 4 (a) presents an existence of high frequency component in the original accelerometer output (thin line). Equation (3) gives a theoretical value of longitudinal oscillation in the anvil.

$$\frac{1}{2L}\sqrt{\frac{E}{\rho}} = 12.3 \text{ (kHz)}. \tag{3}$$

L stands for a longitudinal length of the anvil. *E* and ρ are Young's modulus and density of the anvil, respectively. From FFT (fast Fourier transform) analysis,

dominant frequency (~11.3 kHz) of the high frequency component is almost equivalent to the theoretical value in Eq. (3). It is estimated that the high frequency component originate in mechanical structure of the anvil. Figure 5 shows peak value dependence of demodulated acceleration and accelerometer output on cut-off frequency under the experimental data in Fig. 4.

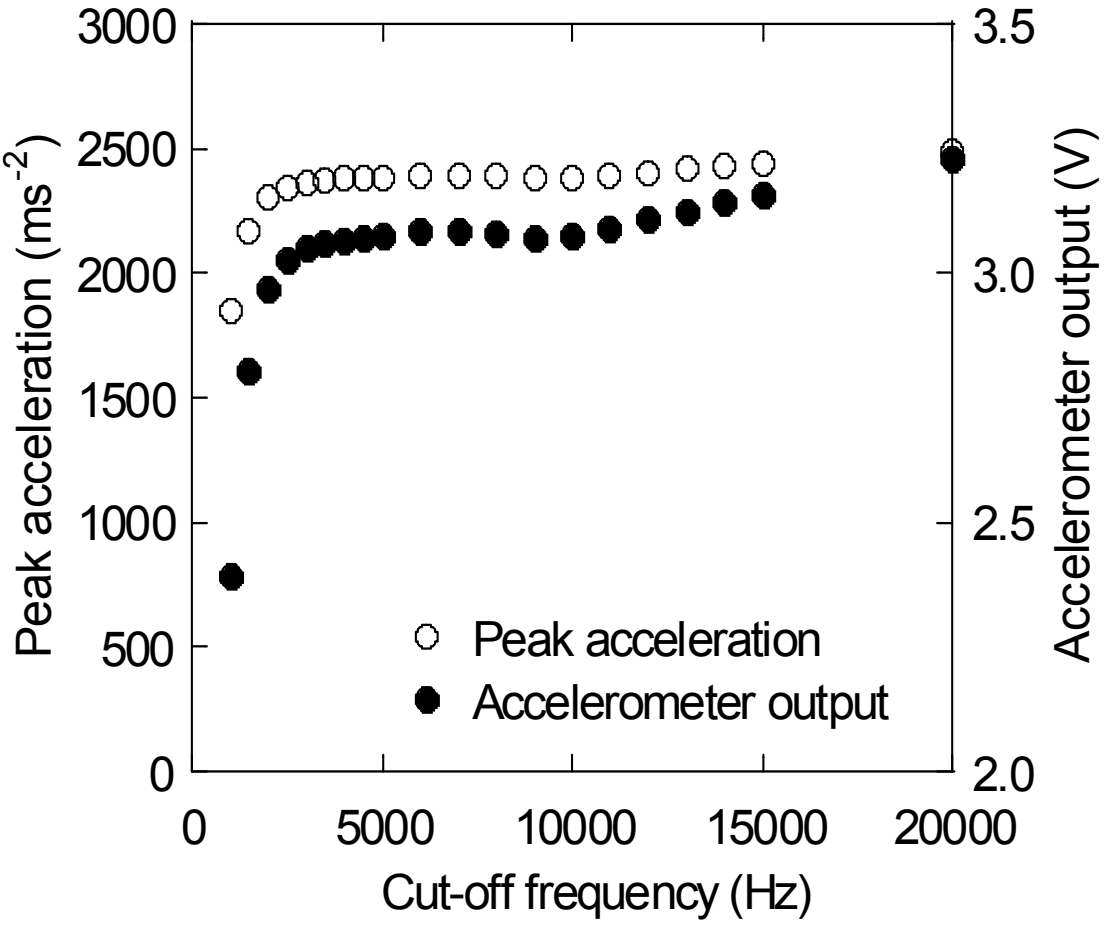

Figure 5 Dependence of peak acceleration and accelerometer sensitivity on cut-off frequency. This result is evaluated from the experimental data in Fig. 4.

Here, each peak value is defined as maximum value in both waveforms. The peak values, particularly accelerometer output, have flat frequency domain from 4000 Hz to 9000 Hz. Since the low-pass digital filter can not suppress the high frequency component more than 9000 Hz, it is difficult to obtain reliable peak value. To optimize cut-off frequency of low-pass digital filter, it is essential to suppress the high frequency component on the longitudinal oscillation indicated in Eq. (3).

Dependence of peak acceleration on rubber hardness in case of aluminum anvil is investigated. (See Fig. 6.)

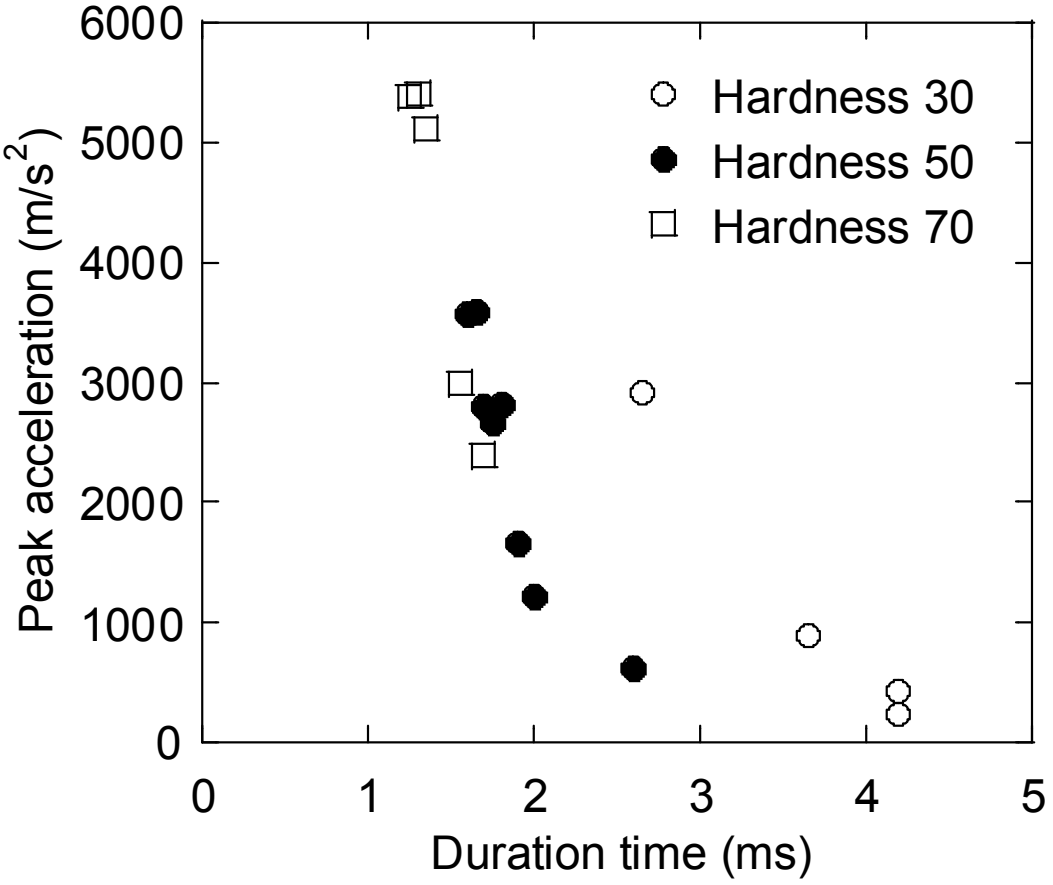

Figure 6 Dependence of peak acceleration on rubber hardness.

From this figure, it is found that the shock exciter in NMIJ satisfies the targeted range (200 m/s^2 to 5000 m/s^2) for shock acceleration calibration. Also, duration time of acceleration waveform seems to be roughly adjustable by using different rubber hardness.

4. Conclusion

Primary calibration machine has been developed for shock acceleration standard from 200 m/s^2 to 5000 m/s^2. In order to generate shock acceleration, two rigid bodies collide inside radial air bearing. Waveform of the shock acceleration was obtained by a combination of a modified Michelson laser interferometer and signal processing, which includes phase unwrapping method, numerical differentiation and low-pass digital filter. Effect of the low-pass digital filtering was investigated to validate phase shift and peak value of the acceleration waveform. To measure accurate accelerometer sensitivity with smaller uncertainty, optimization of low-pass

digital filtering is one of significant issues. For shock acceleration calibration, standardized conditions of low-pass digital filtering shall be discussed in future.

5. Acknowledgement

The authors thank Mr. Yong Bong Lee and his colleagues in KRISS for their help in a design of calibration machine in NMIJ.

References

[1] T. Usuda, A. Ohta, T. Ishigami, O. Fuchiwaki, D. Misaki, H. Aoyama and S. Sato, The current progress of measurement standards for vibration in NMIJ/AIST, Proc. of SPIE (6th International Conference on Vibration Measurement by Laser Techniques), Vol.5503, pp.30-38, 2004.

[2] National Highway Traffic Safety Administration, Document 49 CER Chapter V (10-1-04 Edition) P520.

[3] ISO 16063-13: Methods for the calibration of vibration and shock transducers Part 13, Primary shock calibration using laser interferometer.

[4] P.L.M. Heydemann, Determination and correction of quadrature fringe measurement errors in interferometers. Applied Optics 20, No.19, pp3382-3384, 1981.